# EFFECT OF SOLDER COMPOSITION, PCB SURFACE FINISH AND SOLDER JOINT VOLUME ON DROP SHOCK RELIABILITY

Shuai Shao[1], Francis Mutuku[1,2], Babak Arfaei, Ph.D.[2], Jim Wilcox, Ph.D.[2]
[1]Binghamton University, SUNY, Binghamton, NY, USA
[2]Universal Instruments Corporation, Conklin, NY, USA

**ABSTRACT**
Drop shock reliability testing was performed on circuit boards assembled with several different lead-free solder alloys including SAC305 (Sn3.0Ag0.5Cu). The solder compositions tested range in Ag content from 0 to 3.0% by weight. Alloys with various secondary alloying elements were also included. All drop test boards were assembled such that the solder paste composition matched that of the BGA solder ball alloy to produce homogeneous solder joints of known compositions. An alternative test board design (not JEDEC standard) was used for this drop test evaluation. The test board contains a centrally located CABGA 256 package (17x17 mm body, 1 mm pitch). The board was designed with soldermask defined pads to minimize the occurrence of pad cratering failure modes in the laminate material. The test package was soldered to the drop board using either BGA or LGA interconnections to explore the effects of solder joint volume. Drop shock events were characterized with acceleration monitoring on the drop table and strain gage measurements on the mounted test boards.

All samples were dropped until electrical failure. Solder joint microstructural analysis was performed on failing parts to establish the failure modes. The dominant failure mode was observed to be solder joint failure, either in the bulk solder or cracking along the interfacial intermetallic compound on the board pad. The effect of alloy silver content on drop reliability is noted. SAC305 solder joints were found to produce the best drop performance of all alloys tested for both BGA and LGA joint formats.

Key words: Drop test, drop reliability, lead-free solder, surface mount technology

## INTRODUCTION

Lead free solder joint reliability in drop shock loading has been a recurring issue in mobile and handheld consumer electronics. Changing solder composition may offer an opportunity to improve joint drop reliability. Low Ag alloys such as SAC105 have for instance been reported to have better drop performance than high Ag alloys such as SAC305 [1-5]. Some investigations suggested that this was because the failure mode changed from solder bulk failure (low Ag) to cracking of the interfacial intermetallic (high Ag) [1-5]. Others attributed it to a dominate failure mode of pad cratering for SAC105 on Cu-OSP, yet for SAC305 on Cu-OSP PCB surface finish failure was due to fracture of the $Cu_6Sn_5$ intermetallic compound (IMC) [6].

Mattila [4] explained that IMC cracking happens when the increased yield strength of the solder at high strain rate limited the strain accommodation provided by plastic deformation in the solder during the shock event. Thus the brittle intermetallic layers failed due to increased stress concentration. Solder bulk failure on the other hand, occurred when solder strength was lower, usually the case for low silver alloys. Large plastic deformation in the solder reduces the overall stress in the connection and leads to a ductile bulk solder failure mode. Other researchers have reported that the strength response of SnAgCu solders may indeed vary by the drop acceleration level, increasing with the higher strain rates of large drop acceleration [3,7].

Tensile or peeling stress plays an important role in solder joint failure during the drop test [8,9]. Typically circuit boards are more flexible than the components attached to them. Considering that laboratory test assemblies are often dropped component side down with rigidly affixed board corners, the outermost solder joints will be under tension when the board flexes downward on initial impact. This tensile stress drives crack propagation of any crack initiated in the corner solder joints or in the underlying laminate. Joints at other locations may similarly fail but the outmost corner joints have the highest probability of producing the first failure.

Tensile test for bulk solder joints was performed at various strain rates and aging times by Luan, et al [9]. Three failure modes of bulk solder were reported: brittle failure, ductile failure and mixed mode failure. Their reported data showed that higher strain rate led to statistically more brittle failure in the interfacial intermetallic compound. Longer aging time resulted in a thicker IMC layer and more brittle failure.

Solder alloys doped with various elements can lead to very different drop shock behavior. The effect of micro alloying elements on failure mechanism is not simple. For example, the effect of the addition of 0.1% Bi in high strain rate failures was dependent on the base alloy [10]. For low Ag alloys (Ag<1%), Bi improved drop shock and ball pull performance while the same Bi addition reduced both attributes for the higher Ag SAC305 alloy.

Recently, new candidate board designs have been proposed as replacements for the JEDEC JESD22-B111 drop test board [11]. Design changes were motivated primarily by concerns that the existing JESD22-B111 configuration does

not provide the same stress distribution for all the components during drop, although some components are mounted symmetrically on board [11]. Attributes of some of the new designs include a single component per board [12], four components per board mounted symmetrically [12] or eight components mounted centro-symmetrically on a round test board [13]. Another advantage of the new designs is that they usually have the board size close to that of hand-held portable devices, which can help provide a more realistic reliability assessment [12].

A common shortcoming of many developed inter-connection reliability models is neglecting changes in failure modes. This makes the overall validity of these models questionable as drop tests producing different failure mechanisms are not simply comparable. This project is intended to study the failure behavior of several solder alloys in drop test. Each alloy is used to assemble LGA and BGA components on either a Cu-OSP surface finish board or an immersion silver surface finish board. The test board used is one redesigned from previous drop test efforts to influence the primary failure mode. Failure rates in drop shock are fitted to Weibull distributions for comparison. Characteristic failure modes for each solder alloy | board finish combination are identified.

## EXPERIMENT PREPARATION

### Test Board Assembly

A revised test board design is used for this study rather than the previously used JEDEC standard drop test board. In the multi-component JEDEC drop test board design, the stress distribution experienced during drop is not identical for all the components making analysis and interpretation of results difficult. The test board used is constructed of 6-layer 370HR laminate material with a body size of 77 x 77 mm. The boards were sourced with either Cu-OSP or immersion Ag surface finish.

The Chip Array BGA256 test component has a body size of 17 x 17 mm. The BGA footprint is full array with solder mask defined pads on a 1.0 mm pitch. The component surface finish is electrolytic NiAu. It is assembled to the test board in either the BGA or LGA (solder paste only) configuration.

The five solder alloys evaluated, in order of decreasing Ag content, are SAC305, SN99CN, SAC105, SAC-M, and SN100C. Solder alloy compositions are listed in Table 1. For those samples evaluated in BGA format, the component ball attach process was performed in the Universal Instruments SMT laboratory using 16 mil (400 μm) spheres. A solder paste print process is used for subsequent assembly of the balled components to the test board using pastes with compositions matching the associated ball alloy. All assemblies are reflowed in a nitrogen environment with a peak temperature of 239°C. LGA components were attached using an analogous paste-only SMT assembly process. Sixteen samples for each combination of solder alloy (five), surfaces finish (two) and joint configuration (two) required the assembly of 320 test boards. Fifteen boards are dropped for each experimental cell with the remaining board allocated for initial microstructure inspection.

**Table 1.** Solder Alloy Compositions

| Alloy | Composition |
|---|---|
| SAC305 | Sn - 3.0Ag - 0.5Cu |
| SN99CN | Sn - 1.1Ag - 0.7Cu - 0.05Ni |
| SAC105 | Sn - 1.0Ag - 0.5Cu |
| SAC-M | Sn - 0.5Ag - 1.0Cu - - 0.03Mn |
| SN100C | Sn - -0.7Cu - 0.05Ni +Ge |

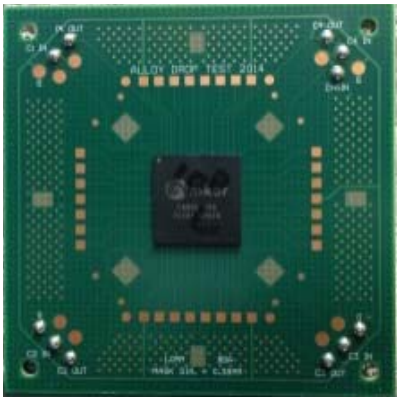

**Figure 1.** Assembled test board (77 mm ×77 mm) with two monitor channels (input, output) accessible at each corner.

### Board Design and Failure Detection

The assembled test board is shown in Figure 1 Each corner of the board has two input channels connecting the outermost corner BGA pad from two sides. In the assembled structure, a continuity monitor signal passes through corner joint A and adjacent joint B into ground as shown in Figure 2. Electric resistance of the input channels to ground is monitored during drop events. If either input 1 or input 2 fails, followed by the other failing after some additional drops, the likely failure mode is pad cratering. It indicates cracks inside the test board laminate propagating from one side to the other severing the two copper traces in sequence. On the other hand, when both channels fail at the same time, solder fatigue in corner joint A or other failure path around adjacent joint B would be the presumed failure mode. Experience indicates that adjacent joint B is unlikely to fail before corner joint A meaning that simultaneous failure of both channels is anticipated to be solder failure in the corner joint (Figure 3). The remaining solder joints in the assembled solder joint array (*i.e.*, beyond the two monitored joints in each corner) are stitched together in a single test net.

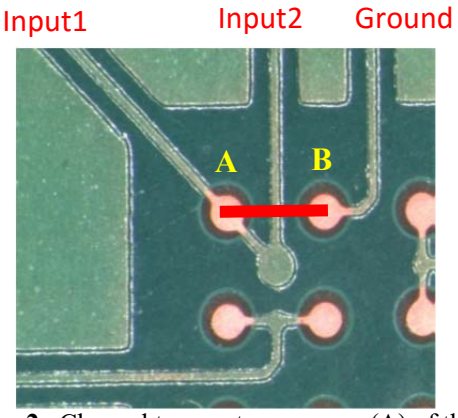


**Figure 2.** Channel traces at one corner (A) of the BGA array. Red line represents the attached component chain. (Image from previous study [14] using NSMD pads.)

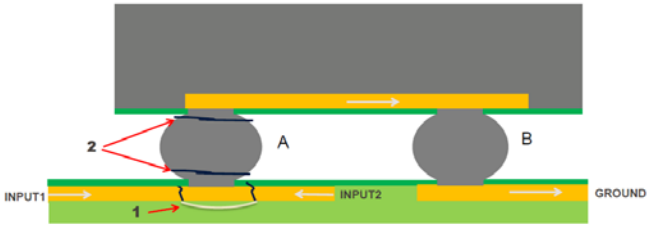


**Figure 3.** Illustration of event detection for failure mode.

A similar board design was used in a previous drop reliability study [14]. Some effects of solder alloy on drop lifetime were observed in that study. However, the dominant failure mode was laminate pad cratering. Shock induced cracks propagated in the board laminate rather than through the solder joints of interest. For an alloy study, it was considered desirable to compare failures occurring in the solder alloys of interest rather than failures in the underlying laminate material. The board design used in this study strengthens copper signal traces and pads as well as uses solder mask defined pads for both component and board side (Figure 4) to promote solder joint failure. Failure is identified by significant increase of electrical resistances through an event detector. While the test circuit is designed to provide some indication of failure mode through event detection, the actual failure mode is always confirmed by cross-sectional observation (Figure 4).

## DROP TEST APPARATUS

Service condition "F" of JEDEC Mechanical Shock Standard (JESD22-B104C) is applied in this study: 900G acceleration peak value, 0.7ms pulse duration, and 386 cm/s (152 in/s) velocity change. The drop test apparatus is a Lansmont shock table illustrated schematically in Figure 5. To expedite testing of the large sample quantities required by this study, mounting fixtures for the simultaneous drop of four test boards were included on the table surface. Each mounting fixture consisted of four standoff posts for the corner mounting holes the board. They were arranged in a two by two array centered on the table.

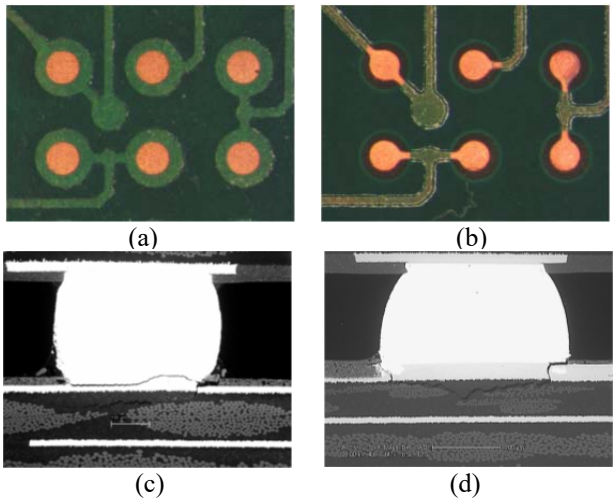


**Figure 4.** (a) Redesigned test board and (c) its failed joint; (b) previous test board and (d) its failed joint.

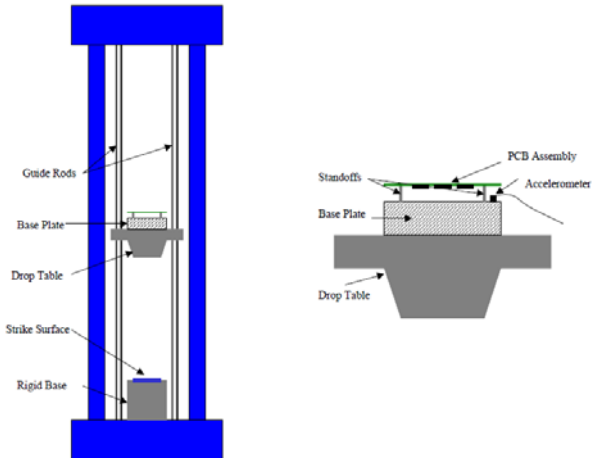


**Figure 5.** Diagram for drop test apparatus and mounting scheme for assembled test board [11]

### Shock Response on Fixture

Shock impulses should be uniformly distributed over the four boards on the drop table. The shock responses on the four fixtures are checked as follows. Fixtures are screwed to the drop table. No boards are mounted, only standoffs. One reference accelerometer keeps the same location on the table for each drop to ensure shock values repeat closely from drop to drop. A second accelerometer is placed on the table surface sequentially at the projected center of each test board location to measure the shock responses during successive drops. Accelerometer readings at the four board locations are plotted in Figure 6. Maximum acceleration values are listed in Table 2. The variation in maxima by location is 1.6% (907G ± 0.8%).

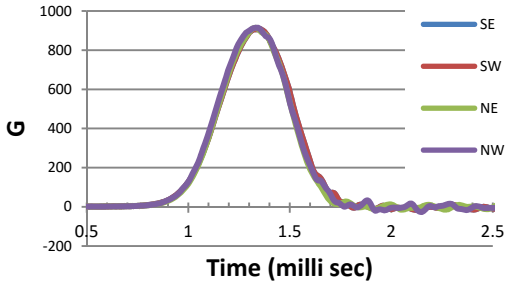


**Figure 6.** Accelerometer readings on the table fixture measured at the projection of each board center.

**Table 2.** Peak table acceleration response by location

| Location | Maximum Response (G) |
|---|---|
| SE | 899.7 |
| SW | 907.6 |
| NE | 914.1 |
| NW | 914.5 |

**Strain Measurement on Board**

Strain gages are mounted at designated solder mask opening locations on the assembled side of the board near the component corners, one gage on each of the four boards mounted. The strain gage locations for each board are shown in Figure 7. Because of a channel count limitation only strains at 45° are measured. Due to the design symmetry these 45° strains are expected to be the principal strains. Samples are dropped with the component facing downward so that the initial drop impact will record board surface tensile strains on each corner.

*Mounting Location Sensitivity*

Mechanical variation (post alignment, washer dimension, etc.) among the four board mounting fixtures on the table may impart some positional dependency in the drop shock impulse. The magnitude of this variation (and thus positional experimental error) is measured through board bending strain measurements during drop events at each mounting position. Four instrumented boards are mounted as shown as Figure 8. Individual strain monitor boards are identified as A, B, C, and D. After one instrumented drop with boards in the initial position shown on the far left, the boards are cycled clockwise to the next mounting position. For example, board A is moved from NW location to NE. Board A is also rotated 90 degrees such that the strain gage orientation will be still be radial, emanating from the center of the table. The other three boards are similarly rotated into new positions. The resultant strain measurements from successive drops are listed in Figure 8 for each of the four unique board placements. Tracking any given board through the four different positions reveals the experimental strain variation. Positional variation exceeds the individual test board variation by an order of magnitude with the NW position consistently producing the highest strain (6% above the overall mean). Individual test boards are consistent to within 1% relative to the overall mean.

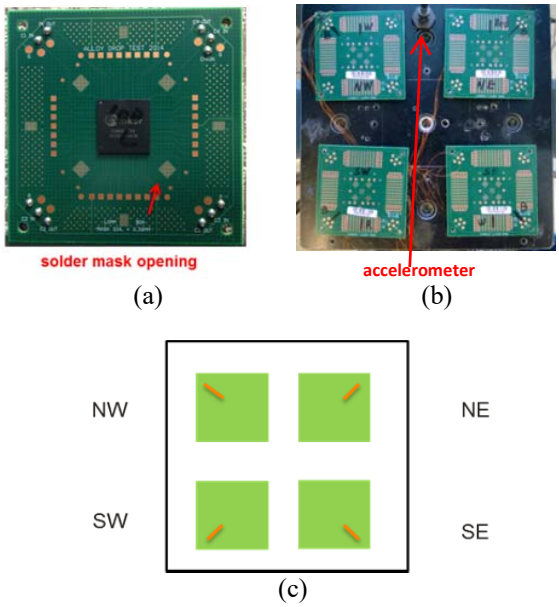


**Figure 7.** (a) Solder mask opening for attaching strain gage, (b) four boards mounted on table with table accelerometer location indicated and (c) board location identifiers

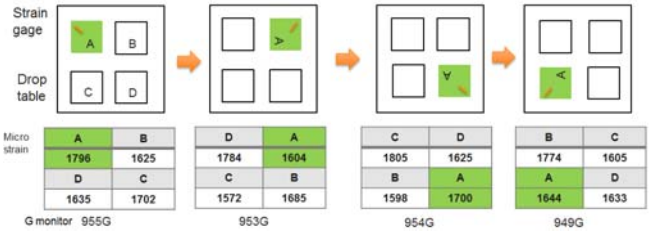


**Figure 8.** Board strain measurement (maximum principal strain, in microstrain) by table mounting position.

**RESULTS AND DISCUSSION**

**Weibull Distribution Plots of BGA Drop Failures**

Figure 9 shows Weibull failure rate distribution plots by solder alloy for drop shock failures with (a) Cu-OSP board surface finish and (b) ImmAg board surface finish. The drop lifetimes indicated are those for the first failing corner on each test board. The SAC105 alloy was limited to eight samples due to yield fallout at assembly.

SAC305 can be seen to be the best performer for both board surface finishes. Noting the variability in drop lifetime (*i.e.*, low Weibull shape factors, β), the other alloys can all be considered to have lower but similar drop performance. In this experiment, the SAC-M alloy on the Cu-OSP finish failed with considerably lower variability than all other experimental cells (β = 8.5).

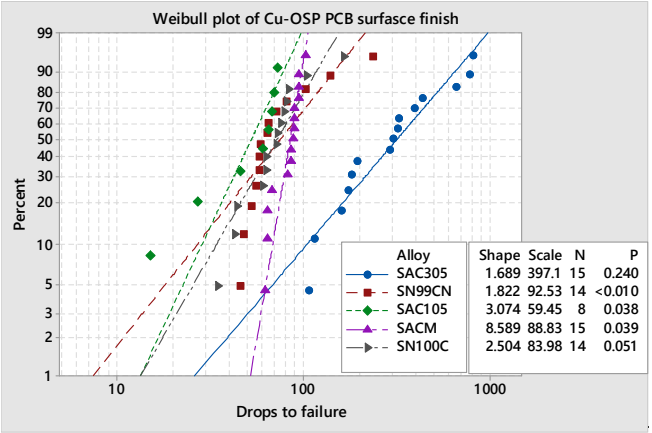


(a)

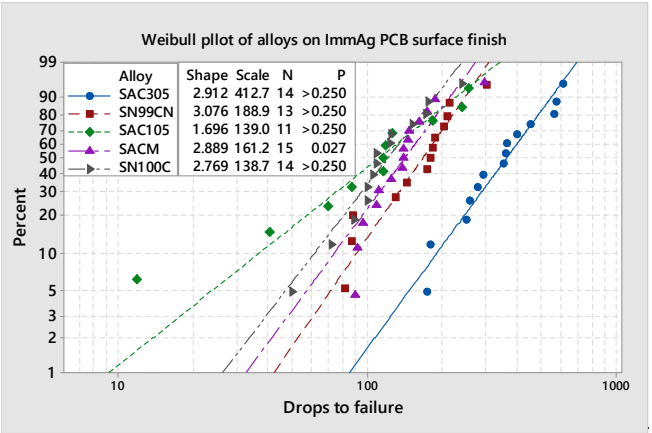


(b)

**Figure 9.** Weibull plots of BGA joints for five alloys on (a) Cu-OSP PCB surface finish (b) ImmAg PCB surface finish

Figure 10 compares the characteristic drop lives of BGA interconnects among the five solder alloys between the two PCB surface finishes. The effect of alloy silver content is seen to be similar for both finishes with the highest silver content (3%, SAC305) showing superior performance and drop lifetime generally decreasing with the silver alloying content. BGA components on ImmAg PCB surface finish uniformly display slightly better drop reliability than those on the Cu-OSP finish.

**Microstructure and Failure Analysis of BGA Joints**

Microstructural analysis was performed for all alloys, both as-reflowed (before drop) and after repetitive drop failure. The assemblies were cross-sectioned along the body diagonal of the board such that the traces of two input channels at the corner pad are visible on either side of the sectioned joint. Metallographic sections are prepared in the usual manner: sequential grinding using 80, 200, 800, 1200, 2000 and 4000 grit SiC papers followed by a final polish with 3μm and 1μm diamond compounds and 0.05μm $Al_2O_3$.

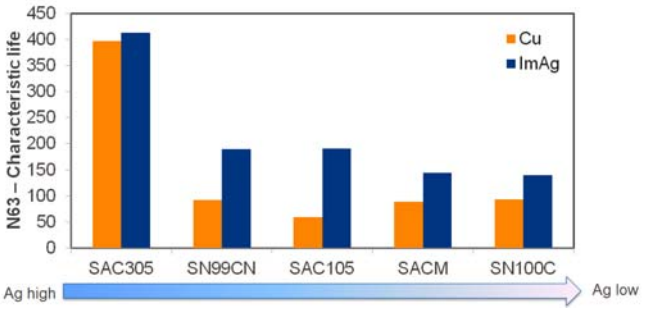


**Figure 10.** Comparison of characteristic drop life of BGA256 components between two surface finishes for the five solder alloys listed in order of decreasing Ag content.

*BGA Failure Modes*

Solder failure is identified during repetitive drop using an event detector to capture excursions of electrical resistance beyond a threshold value. Failure is declared when three such events are observed within five consecutive drops. The drop test of each assembly is stopped after its first failure was confirmed. In 95% of samples, a corner joint was found to fail first. Metallographic samples are oriented such the failed corner joint is viewed on the right side of the cross-section, the component on the top side of the image and the circuit board on the bottom. The opposite corner joint (not yet failed) will then be visible in the far left side of the section.

Figure 11 shows a representative image of one of the drop failure modes observed: pad cratering beneath the BGA pad. One can see in Figure 11a a complete crack traversing from one side of the joint to the other in the PCB laminate structure beneath the pad. There is also a shorter crack visible on the left, inside IMC layer. The inner side and outer side labeled in Figure 11a refer, respectively, to the side nearest the center of the package and side away from the package corner. The crack within the IMC layer initiates from the inner side of the corner joint (Fig. 11b), while the PCB laminate crack initiates from outer side of the corner joint. The SEM image of Figure 11c reveals the connecting crack between the two competing crack paths producing the electrical failure.

Figure 12 shows a different joint with a similar laminate crack emanating from the outer sider the joint and propagating under the pad. It has not yet propagated through the joint to produce a failure. A second BGA failure mode also observed: a combination IMC/solder failure. A complete through crack is seen to propagate in the solder as well as along the interfacial IMC. Since this IMC/solder crack has fully transected the joint, the direction of propagation is not obvious simply from this image.

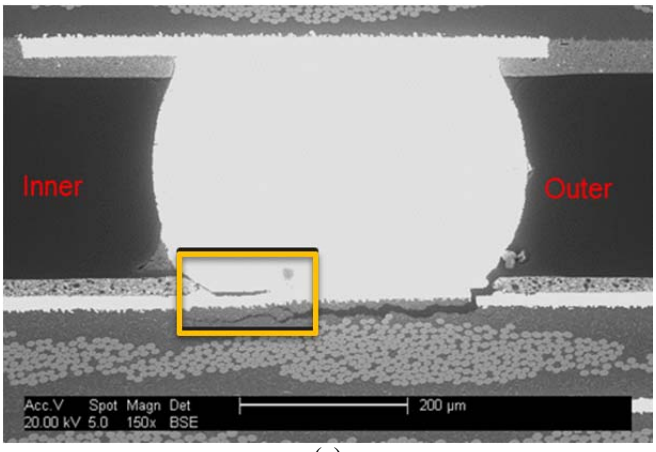


(a)

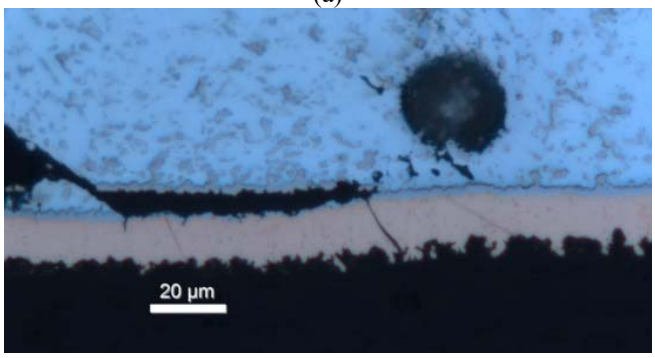


(b)

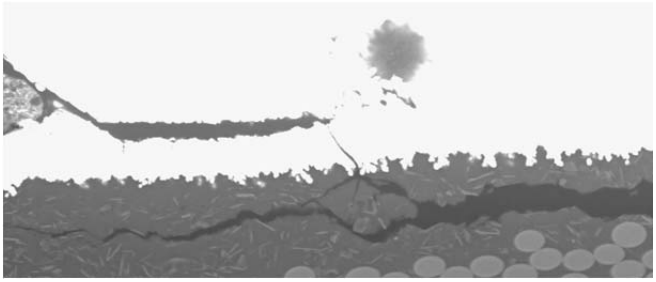

(c)

**Figure 11.** Pad cratering failure mode: (a) full BGA view, (b) the local region of IMC cracking, and (c) SEM image of the same local area showing PCB laminate cracking.

The characteristic starting location for this failure mode however can be determined from the symmetrical opposite corner joint where the failure process is not yet complete. This joint is shown in Figure 13. Here, the outer side will be to the left of the joint. This joint has not yet failed and none of the visible cracks are complete. Again, a laminate crack can be observed starting from outer side of the corner joint and propagating under the pad. There is also a crack propagating along the interface solder joint IMC similar to that observed in the opposite corner joint. This IMC crack is not complete and thus can be clearly seen to emanate from the right (inner) side of the joint (detail shown in Figure 13b). The left side detail image in Figure 13c confirms the IMC/solder cracking process is yet incomplete.

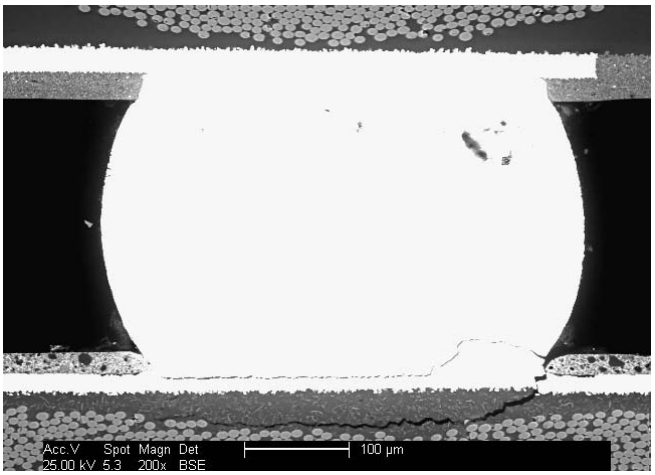


**Figure 12.** BGA failure mode: IMC/solder failure

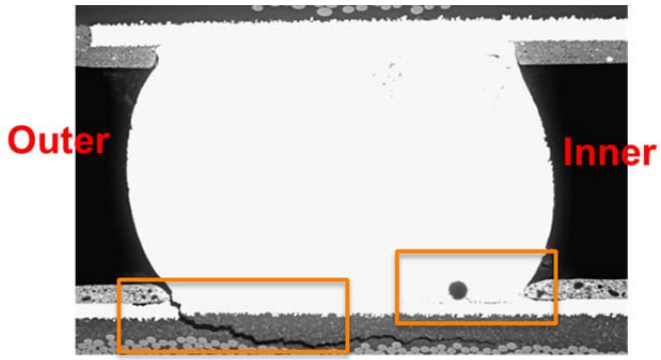


(a)

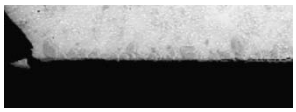

(b)

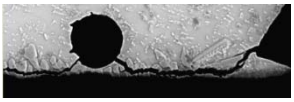

(c)

**Figure 13.** Crack in a non-failed BGA corner joint (a) whole cross-section (b) local area of high magnitude on the left (c) local area of high magnitude on the right

From the above analysis, we see that two distinct cracking mechanisms are competing to produce interconnect failures in this BGA256 component. These alternate crack paths, shown schematically for a corner joint in Figure 14, arise from the oscillating flexure of the board after initial impact. Board flexure from the initial drop impact imposes a tensile load on the 'outer' side of the joint at the base of the BGA pad, initiating and propagating a crack into the laminate. The upward rebound board flexure then imposes a tensile impulse on the 'inner' side of the BGA pad and compression on the outer side. The magnitude of the second impulse is necessarily smaller than the initial impact loading. The magnitude of the rebound flexure is reduced through dampening. Moreover, the board cannot flex away from the plane of the package on the inner side as readily as it can on the outer side because the inner side board is constrained by the adjacent solder joints attached to the package above. That's not to say however the outer crack will always preferentially produce a failure. Different levels

of fracture toughness are encountered along the two crack paths as well as different path lengths being required to produce a failure. Depending on solder alloy and interfacial toughness considerations either the solder/IMC crack path or the laminate crack path under the pad may win out, transecting the interconnect to produce an electrical open.

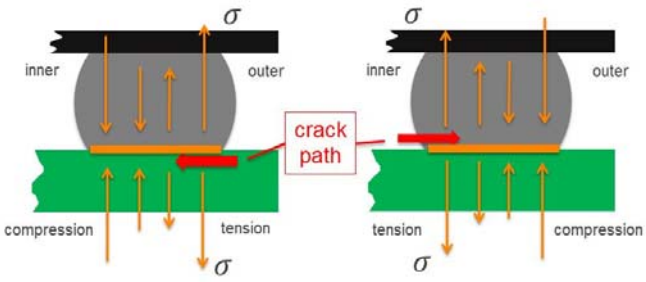


**Figure 14.** Illustration of crack path competition in corner BGA solder joints due to cyclic oscillations after drop. Stresses due to (a) downward board deflection at initial drop impact and (b) upward rebound deflection.

For certain alloy:finish combinations, pad cratering proved to be a relatively common failure mode. In these instances, the laminate crack shown in the diagonal cross-section of Figures 11 – 13 propagated to meet another opposing laminate crack from the other direction. When viewed from a section taken in the plane of board ('Z-section') this failure mode is characterized by a circular crack propagating into the plane of the BGA pad from the perimeter of the solder mask opening until the central laminate crater separates from the pad. An example is shown in Figure 15. All pad cratering events that produced electrical failures did so with such circular cracks through the BGA pad. No failures through the input copper traces were observed. This mode of circular pad cratering causes the two input channels appear to be open simultaneously (see Figure 3), the same failure signature as the IMC/solder failures. Thus, the event detector could detect failure but not uniquely identify the failure mode as anticipated. All failures must be cross-sectioned to identify the failure mode.

The observed failure modes of the BGA256 package in 900G drop shock are summarized in Table 3 for all solder alloys tested. For each alloy:finish combination, the failure modes were sampled at three different places in the failure rate distribution: early failure, characteristic life failure ($N_{63}$) and late failure. The early and late failure cases examined samples that failed with the shortest and longest drop lifetime, respectively. For $N_{63}$, samples that failed nearest the characteristic life of the Weibull distribution fit are selected. From Table 3, one can see that more pad cratering failures occur for BGA joints with the ImmAg PCB surface finish than those with Cu-OSP finish. In general, the combined IMC/solder failures tend to produce shorter drop lifetimes than pad cratering failures. It is interesting to note that the lowest variability case (SAC-M on Cu-OSP) produced only IMC/solder failures.

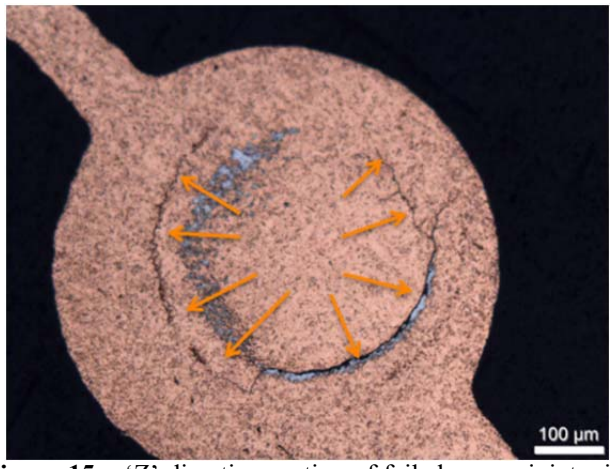


**Figure 15.** 'Z' direction section of failed corner joint with pad cratering

**Table 3.** Failure Modes of BGA256 in Drop

| BGA | Failure Mode | | | | | |
|---|---|---|---|---|---|---|
| | Cu-OSP | | | ImmAg | | |
| | Early | N63 | Late | Early | N63 | Late |
| SAC305 | IMC/solder | Pad cratering | Pad cratering | IMC/solder | IMC/solder | IMC/solder |
| SN99CN | IMC/solder | IMC/solder | Pad cratering | Pad cratering | Pad cratering | Pad cratering |
| SAC105 | Pad cratering | IMC/solder | IMC/solder | IMC/solder | Pad cratering | Pad cratering |
| SAC-M | IMC/solder | IMC/solder | IMC/solder | Pad cratering | IMC/solder | Pad cratering |
| SN100C | IMC/solder | Pad cratering | IMC/solder | Pad cratering | Pad cratering | Pad cratering |

**Weibull Distribution Plots of LGA Drop Failures**

Weibull distributions fits of drop test life of LGA assemblies for five solder alloys on two PCB surface finishes are shown in Figure 16. LGA joints with the SAC305 alloy show the best performance on Cu-OSP PCB surface finish. On immersion Ag boards however, LGA joints of the SN99CN and SN100C alloys are seen to have the best drop performance.

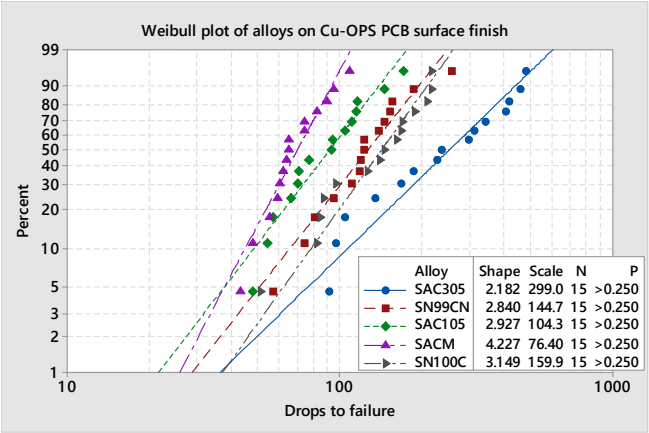


(a)

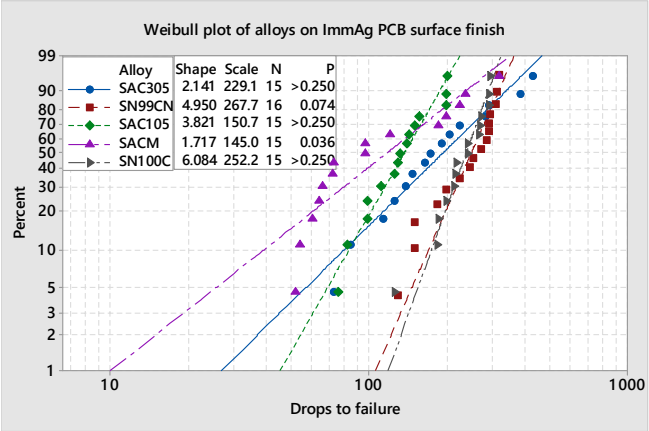


(b)

**Figure 16.** Weibull distribution plots of LGA joints failures in drop for five solder alloys on (a) Cu-OSP PCB surface finish and (b) ImmAg PCB surface finish

Figure 17 compares the characteristic drop lives of LGA interconnects for five solder alloys on two finishes from the Weibull fits of Figure 16. With the notable exception of SAC305, the drop life of LGA joints on ImmAg is greater than that of LGA joints on Cu-OSP. Observed failure modes provide some insight into these relative behaviors.

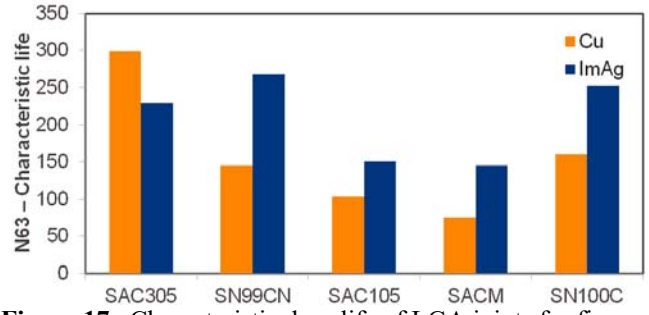


**Figure 17.** Characteristic drop life of LGA joints for five alloys and two PCB surface finishes. Alloys listed in order of decreasing Ag content.

*LGA Failure Modes*

The failure modes observed in LGA solder joints at different relative drop lifetimes are listed in Table 4. For LGA joints on Cu-OSP finish, all drop failures exhibit bulk solder failure (see for example, Figure 18). This failure mode was not observed in the larger volume BGA solder joints for any alloy. For LGA joints on ImmAg finish, IMC failure, IMC/solder mixed failure, pad cratering and bulk solder failures are all observed. Representative images of each are shown in Figure 19. It is noted that in all the failed LGA joints on ImmAg PCB surface finish, cracks were observed in the PCB laminate under the pad. Partial pad cratering always happened regardless of the crack path producing the ultimate interconnect failure. These competitive cracking modes dissipate additional drop shock energy and may in some instances serve to prolong the drop lifetime of LGA over BGA. For LGA joints failing through the bulk solder (primarily those on OSP), greater solder Ag content was seen to correlate with better drop performance in these SnAgCu based alloys, presumably due to the increased strength of solder (see Figure 20a).

**Table 4.** Failure Modes of LGA256 in Drop

| LGA | Failure Mode | | | | |
|---|---|---|---|---|---|
| | Cu-OSP | | ImmAg | | |
| | Early | Late | Early | N63 | Late |
| SAC305 | Bulk | Bulk | IMC | IMC/solder | Pad cratering |
| SN99CN | Bulk | IMC/solder<br>Pad crater | IMC/solder | IMC/solder | Pad cratering |
| SAC105 | Bulk | Bulk | Bulk | IMC/solder | Bulk |
| SAC-M | Bulk | Bulk | Bulk | Bulk | Pad Cratering |
| SN100C | Bulk | Bulk | Bulk | Bulk | Bulk |

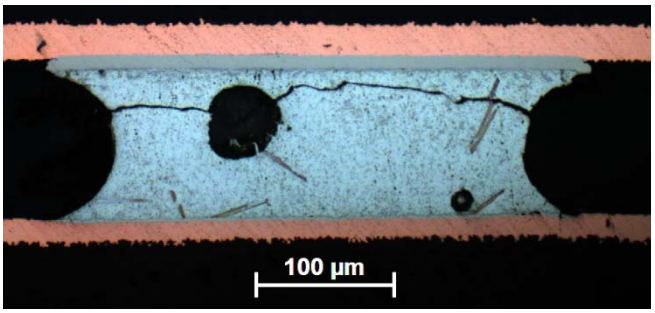


**Figure 18**. Representative failure mode for bulk solder failure of LGA joints on Cu-OSP PCB surface finish.

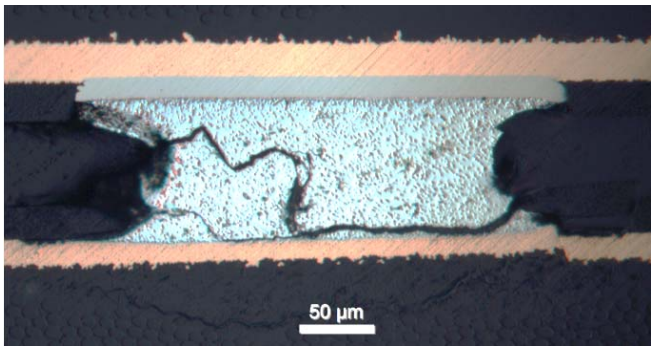


(a)

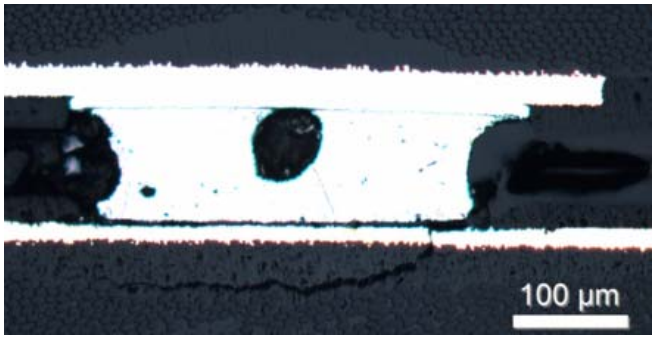


(b)

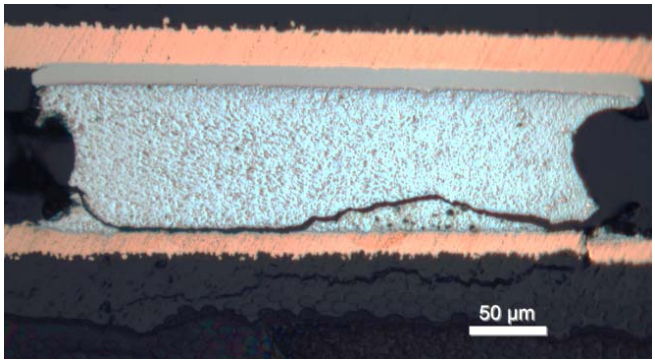


(c)

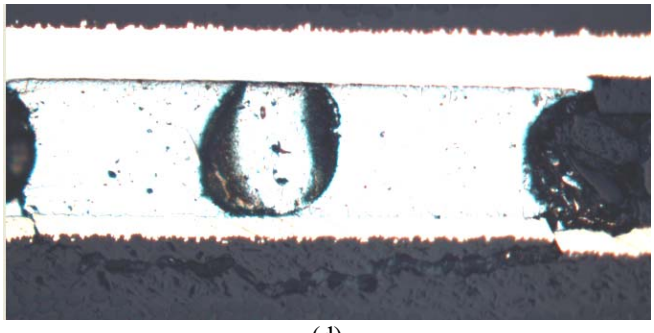

(d)

**Figure 19.** LGA failure modes on ImmAg PCB surface finish: (a) solder bulk failure, SN100C, late (b) IMC failure, SAC305, early (c) IMC/solder mixed failure, SAC105, early (d) pad cratering, SAC305, late

**Solder Joint Volume Effects: BGA vs. LGA**

The characteristic drop lifetimes of LGA and BGA solder joints are compared in Figure 20 for each board finish. No obvious trend in effect of joint type and solder alloy is apparent, although for any given alloy the relative performance between these joint configurations is mostly reproducible across the two surface finishes used. SN99CN and SN100C perform better in the LGA format while SAC305 and SAC-M perform better in the BGA format. SAC105 performs better in the lower volume LGA joints on Cu-OSP finish but is insensitive to solder joint volume on the immersion Ag finish.

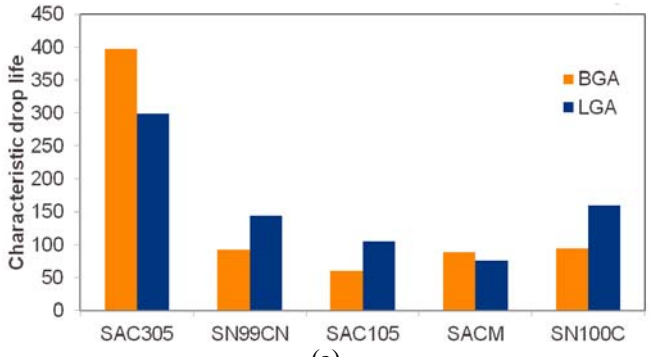


(a)

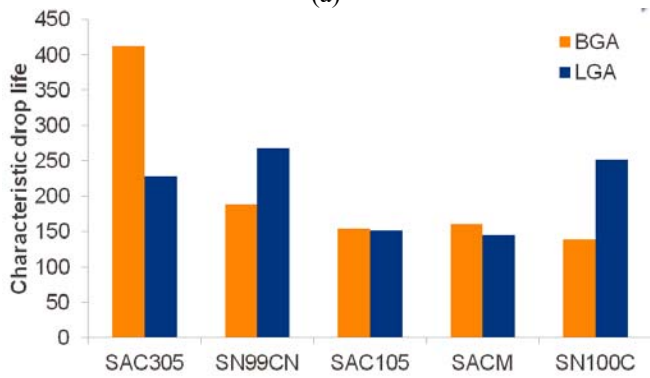


(b)

**Figure 20.** Comparison of characteristic life between BGAs and LGAs on (a) Cu-OSP PCB surface finish (b) ImAg PCB surface finish

**SUMMARY AND CONCLUSIONS**

Five Pb-free solder alloys on two PCB surface finishes were evaluated for drop shock reliability with two different solder joint volumes (LGA and BGA). Using a drop test board specifically designed to promote solder joint failures (*i.e.*, solder mask defined board pads), the following experimental observations were made.

Of the five solder alloys evaluated, SAC305 performs the best, or nearly so, for all test conditions (board finish and solder joint volume). SN99CN is generally the second best drop performer with SN100C performing very similarly. In the BGA joint configuration, SAC-M is characterized by notably low variability in drop lifetime when used on Cu-OSP finish boards. On immersion Ag boards or in the LGA configuration, its failure rate variability is more typical.

Repetitive drop shock testing was seen to produce four distinct interconnect failure modes: bulk solder failure,

interfacial IMC failure, mixed IMC/solder failure and laminate pad cratering. Different failure mode trends were observed between BGA and LGA joints. Board surface finish also played a role in determining failure mode. On Cu-OSP surface finish, SAC305 BGA joints showed mainly pad cratering failure while BGA joints of other alloys generally showed mixed IMC/solder failure. On the ImmAg finish, the results were roughly reversed; BGA joints of SAC305 showed IMC/solder failure while other alloys mostly produced pad cratering failures.

LGA joints on the Cu-OSP finish produced mainly bulk solder failures. On the ImmAg finish however, LGA joints produced examples of all four failure modes with the low Ag alloys tending to have more solder bulk failure. For BGA joints on ImmAg, alloys with lower Ag amount tended to have more pad cratering. Pad cratering failure was in general more prevalent on the ImmAg finish.

Given the integral involvement of the laminate in the drop shock failure process, the observations and conclusions made in this study should be considered applicable only to the laminate material and pad design used. If a more robust laminate formulation further suppresses the pad cratering mechanism, more solder and interfacial failures would be observed, perhaps altering the observed relative performance the alloys.

**ACKNOWLEDGEMENTS**

This investigation was motived by the interests of member companies in the AREA Consortium hosted by Universal Instruments Corporation. The authors gratefully acknowledge consortium funding provided for its execution.

**REFERENCES**

1. Farris, A., *et al*, "Impact Reliability of Edge-Bonded Lead-Free Chip Scale Packages," *Microelectronics Reliability*, Vol. 49, Issue 7, 2009
2. Karppinen, J., *et al*, "Shock impact reliability characterization of a handheld product in accelerated tests and use environment," *Microelectronics Reliability*, Vol. 52, Issue 1, 2012
3. Suh, Daewoong, *et al*, "Effects of Ag content on fracture resistance of Sn–Ag–Cu lead-free solders under high-strain rate conditions," *Mater Sci Eng A*, Vol. 460–461, 2007
4. Mattila, T.T. and Kivilahti, J.K., "Failure Mechanisms of Lead-Free Chip Scale Package Interconnections under Fast Mechanical Loading," *Journal of Electronic Materials*, Vol. 34, Issue 7, 2005
5. Syed, A., *et al*, "Alloying effect of Ni, Co, and Sb in SAC solder for improved drop performance of chip scale packages with Cu OSP pad finish," *Proc. Electronic Components and Technology Conference*, 2006
6. Roggeman, B., "Comparison of Drop Reliability of SAC105 and SAC305 on OSP and ENIG Pads," *Unovis Area Array Consortium*, 2007
7. Mattila, T.T., *et al*, "The Reliability of Micro-alloyed Sn-Ag-Cu Solder Interconnections under Cyclic Thermal and Mechanical Shock Loading," *Journal of Electronic Materials*, Vol. 43, Issue 11, 2014
8. Zhou, T. and Fan, X., "Effect of System Design and Test Conditions on Wafer Level Package Drop Test Reliability," *SMTA International Proceedings*, 2013
9. Luan, J., *et al*, "Dynamic responses and solder joint reliability under board level drop test," Micro-electronic Reliability, 2007
10. An, T. and Qin, F., "Effects of the intermetallic compound microstructure on the tensile behavior of Sn3.0Ag0.5Cu/Cu solder joint under various strain rates," Microelectronics Reliability, 2014
11. JEDEC solid state technology association, "Board Level Drop Test Method of Components for Handheld Electronic Products," 2003
12. Lall, P., *et al*, "Transient Dynamics Model and 3D-DIC Analysis of New-Candidate for JEDEC JESD22-B111 Test Board," *Proc. Electronic Components and Technology Conference*, 2014
13. Liu, F., *et al*, "Experimental and numerical analysis of BGA lead-free solder joint reliability under board-level drop impact," *Microelectronics Reliability*, 2008
14. Joshi, Gaurang, Arfaei, Babak, "Effect of Solder Alloy on Drop Test Performance of LGAs and BGAs," *AREA Consortium Report, 2014*